Journal of Power Sources 196 (2011) 5873–5880

Contents lists available at ScienceDirect

Journal of Power Sources

journal homepage: www.elsevier.com/locate/jpowsour

Constrained model predictive control of a solid oxide fuel cell based on genetic optimization

Yiguo Li*, Jiong Shen, Jianhong Lu

Department of Energy Information and Automation, Southeast University, 2 Sipailou, Nanjing 210096, China

ARTICLE INFO

Article history:
Received 4 March 2011
Accepted 4 March 2011
Available online 11 March 2011

Keywords:
Solid oxide fuel cell
Model predictive control
Support vector machine
Genetic algorithm
Terminal cost

ABSTRACT

Solid oxide fuel cells (SOFCs) are considered to be among the most important fuel cells. However, SOFCs present a challenging control problem owing to their slow dynamics, nonlinearity, and tight operating constraints. In this paper, we propose a model predictive control (MPC) strategy based on genetic optimization to solve the SOFC control problem. First, a support vector machine (SVM) model is identified to approximate the behavior of the SOFC system, then a specially designed genetic algorithm (GA) is employed to solve the resulting constrained nonlinear predictive control problem. A terminal cost is incorporated into the standard performance index to further enhance the control performance. Moreover, the GA is accelerated by improving the initial population based on the optimal control sequence obtained for the previous sampling period and a local controller. In addition, a dynamic constraint is also adopted in order to meet the requirements for the desired fuel utilization and control constraints. The measures to achieve offset-free properties are also discussed. Simulation results on an SOFC system illustrate that the proposed method can successfully deal with the control and control move constraints, and that a satisfactory closed-loop performance can be achieved.

1. Introduction

Solid oxide fuel cells (SOFCs) are considered to be among the most important fuel cells. Among the various types of fuel cell, solid oxide fuel cells (SOFCs) have attracted considerable interest as they offer a wide range of applications, flexibility in the choice of fuel, high system efficiency, etc. [1]. However, SOFCs present a challenging control problem owing to their slow dynamics, nonlinearity, and tight operating constraints [2].

Model predictive control (MPC) appears to be the most appropriate control strategy for SOFCs. A comparable H_∞ control strategy for an SOFC model has been shown to be unsatisfactory [2]. Recently, a data-driven linear MPC strategy using subspace system identification was proposed in Ref. [3] to control an SOFC system. However, more researchers have resorted to nonlinear MPC strategies for better control performance [4–9]. These studies have typically employed nonlinear models, such as the Hammerstein model or the radial basis function (RBF) neural network model, as predictors, and then a non-deterministic polynomial–time hard (NP-hard) nonlinear optimization problem was solved on-line using conventional nonlinear optimization techniques, e.g. sequential quadratic programming (SQP). In contrast to these studies, genetic algorithm (GA)-based MPC has been widely studied in recent years because GAs have a number of advantages over conventional nonlinear optimization techniques in solving the constrained nonlinear optimization problem [10–15].

In this paper, we propose a constrained MPC strategy to solve the SOFC control problem based on a support vector machine (SVM) and genetic optimization. A terminal cost is incorporated into the standard performance index to make it possible to adopt short horizons while maintaining a satisfactory performance. Moreover, specially designed genetic operators are employed to make the newly generated chromosomes satisfy the constraints automatically, and the GA is accelerated by improving the initial population based on the optimal control sequence obtained at the previous sampling period and a local controller. In addition, the measures to achieve offset-free properties are also discussed.

The paper is organized as follows: Sections 2 and 3 introduce the SOFC system and some points that need to be considered for the design of a controller. Section 4 gives a brief introduction to the SVM. Constrained nonlinear predictive controller design using GA optimization is presented in Section 5. The simulations and discussions are presented in Section 6. This is followed by the conclusion in Section 7.

2. SOFC system description

The SOFC system includes a fuel processing unit or reformer and a fuel cell stack. Hydrogen is the main fuel for most types of fuel cell. Nevertheless, other fuels, such as methane, methanol, ethanol,

* Corresponding author. Tel.: +86 25 83795951x804; fax: +86 25 83795951x801.
E-mail address: lyg@seu.edu.cn (Y. Li).

0378-7753/$ – see front matter © 2011 Elsevier B.V. All rights reserved.
doi:10.1016/j.jpowsour.2011.03.010

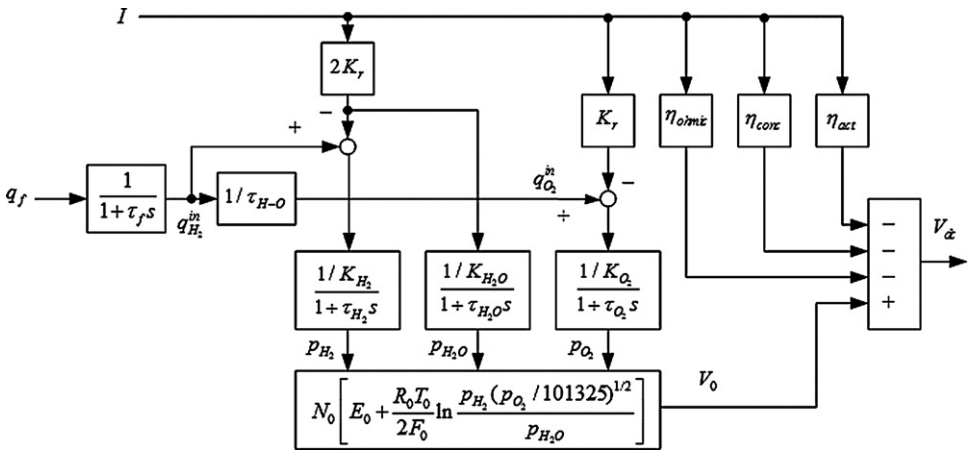

Fig. 1. SOFC system dynamic model.

gasoline, and oil derivatives, can also be used when a reformer is included in a fuel cell system for converting the fuel into hydrogen.

The basic components of an SOFC are the anode, the cathode, a ceramic electrolyte, and two ceramic electrodes. In a fuel cell, fuel is supplied to the anode and air is supplied to the cathode. At the cathode–electrolyte interface, oxygen molecules accept electrons from the external circuit to form oxide ions. The electrolyte layer allows only oxide ions to pass through it, and at the anode–electrolyte interface, hydrogen molecules present in the fuel react with oxide ions to form steam with the release of electrons. These electrons pass through the external circuit and reach the cathode–electrolyte layer, and thus the circuit is closed.

In this paper, a widely accepted dynamic model of an SOFC system is adopted [2–7], as shown in Fig. 1, where V_{dc} denotes the stack output voltage (V), q_f the natural gas flow rate (mol s^{-1}), and I the external current load (A); p_{H_2}, p_{O_2}, and p_{H_2O} denote the partial pressures of hydrogen, oxygen, and water (Pa), respectively; and $q^{in}_{H_2}$ and $q^{in}_{O_2}$ are the input flow rates of hydrogen and oxygen (mol s^{-1}), respectively. Table 1 contains the parameters of the SOFC model [2].

Applying Nernst's equation and taking into account ohmic, concentration, and activation losses (i.e., η_{ohmic}, η_{conc}, and η_{act}), the stack output voltage is represented as follows by applying Laplace transforms [2–7]:

$$V_{dc} = V_0 - \eta_{act} - \eta_{ohmic} - \eta_{conc} \tag{1}$$

Table 1
Parameters in the SOFC system.

Parameter	Value	Unit	Representation
T_0	1273	K	Absolute temperature
F_0	96,485	C mol^{-1}	Faraday's constant
R_0	8.314	J mol^{-1} K^{-1}	Universal gas constant
E_0	1.18	V	Ideal standard potential
N_0	384	–	Number of cells in series in the stack
K_r	0.996×10^{-3}	mol s^{-1} A^{-1}	Constant, K_r=N_0/4F_0
K_{H_2}	8.32×10^{-6}	mol s^{-1} Pa^{-1}	Valve molar constant for hydrogen
K_{H_2O}	2.77×10^{-6}	mol s^{-1} Pa^{-1}	Valve molar constant for water
K_{O_2}	2.49×10^{-5}	mol s^{-1} Pa^{-1}	Valve molar constant for oxygen
τ_{H_2}	26.1	s	Response time of hydrogen flow
τ_{H_2O}	78.3	s	Response time of water flow
τ_{O_2}	2.91	s	Response time of oxygen flow
τ_{H-O}	1.145	–	Ratio of hydrogen to oxygen
r	0.126	Ω	Ohmic loss
τ_f	5	s	Time constant of the fuel processor
∂	0.05	–	Tafel constant
β	0.11	–	Tafel slope
I_L	800	A	Limiting current density

$$V_0 = N_0 \left[E_0 + \frac{R_0 T_0}{2F_0} \ln \frac{p_{H_2}(p_{O_2}/101,325)^{1/2}}{p_{H_2O}} \right] \tag{2}$$

where

$$p_{H_2} = \frac{1/K_{H_2}}{1+\tau_{H_2} s} \left(\frac{1}{1+\tau_f s} q_f - 2K_r I \right) \tag{3}$$

$$p_{O_2} = \frac{1/K_{O_2}}{1+\tau_{O_2} s} \left(\frac{1/\tau_{H-O}}{1+\tau_f s} q_f - K_r I \right) \tag{4}$$

$$p_{H_2O} = \frac{1/K_{H_2O}}{1+\tau_{H_2O} s} 2K_r I \tag{5}$$

$$\eta_{ohmic} = Ir \tag{6}$$

$$\eta_{act} = \partial + \beta \ln I \tag{7}$$

$$\eta_{conc} = -\frac{R_0 T_0}{2F_0} \ln \left(1 - \frac{I}{I_L} \right) \tag{8}$$

3. Design considerations for an SOFC system

The following aspects should be considered in the design of a controller for the SOFC system:

(1) A nonlinear controller is preferred over a linear controller because of the nonlinearity of the SOFC in response to a change of operating points. The stationary voltage/current characteristics of an SOFC system are depicted in Fig. 2, which shows that the SOFC exhibits nonlinear behavior over a wide operating regime. The stack voltage usually shows significant changes, especially at low and high current loads, and an overloaded current leads to a rapid deterioration of the operating stack voltage.
(2) As a measurable disturbance, the current load I should be utilized to construct a feedforward loop to keep the output voltage steady by speeding up the initial response of fuel flow to drastic current changes.
(3) Besides ordinary actuator constraints on the control signal, the fuel utilization of the SOFC system should also be kept within a safe range for as long as possible. Fuel utilization is one of the most important operating variables that can affect the performance of an SOFC. Fuel utilization is defined according to Eq. (9):

$$u_f = \frac{q^{in}_{H_2} - q^{o}_{H_2}}{q^{in}_{H_2}} = \frac{q^{r}_{H_2}}{q^{in}_{H_2}} = \frac{2K_r I}{q^{in}_{H_2}} \tag{9}$$

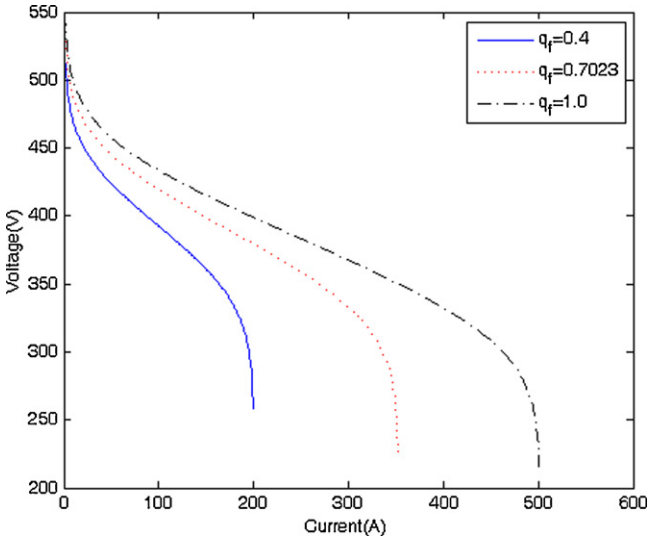

Fig. 2. Voltage–current characteristics of an open-loop SOFC under different fuel flow conditions.

where $q^{in}_{H_2}$, $q^{o}_{H_2}$, and $q^{r}_{H_2}$ are the hydrogen input, output, and reacted flow rates, respectively. The desired range of fuel utilization is from 0.7 to 0.9. This is in order to prevent overused and underused fuel conditions; an overused-fuel condition can lead to permanent damage to the cells due to fuel starvation, while an underused-fuel situation results in low efficiency of the SOFC [3–6].

4. Support vector machine

This section briefly reviews the ε-SVM algorithm [16,17].

Consider the training data set $D = \{\boldsymbol{x}_i, y_i\}_{i=1}^m$, where $\boldsymbol{x}_i$ is the ith input data in the input space $\mathbb{R}^n$ and $y_i \in \mathbb{R}$ is the corresponding output value. The SVM approximates the relationship between the input and output data points in the following form:

$$F(\boldsymbol{x}_i) = \langle \boldsymbol{w}, \phi(\boldsymbol{x}_i) \rangle + b \tag{10}$$

where $\boldsymbol{w}$ is a vector in the feature space $F \subseteq \mathbb{R}^n$, $\phi(\boldsymbol{x}_i)$ is a mapping from the input space to the feature space F, b is the bias term, and $\langle ., . \rangle$ denotes the inner product in F.

The ε-SVM model is aimed at minimizing the loss function $\frac{1}{2}\|\boldsymbol{w}\|^2 + (C/m)\sum_{i=1}^m |y_i - F(\boldsymbol{x}_i)|_\varepsilon$ based on the following ε-insensitive model:

$$|y_i - F(\boldsymbol{x}_i)|_\varepsilon = \max\{0, |y_i - F(\boldsymbol{x}_i)| - \varepsilon\} \tag{11}$$

The optimization problem can be formulated as:

$$\min \; J(\boldsymbol{w}, b, \xi_i^+, \xi_i^-) = \min_{\boldsymbol{w}, b, \xi_i^+, \xi_i^-} \frac{1}{2}\|\boldsymbol{w}\|^2 + \frac{C}{m}\sum_{i=1}^m (\xi_i^+ + \xi_i^-) \tag{12}$$

$$s.t. \begin{cases} y_i - \langle \boldsymbol{w}, \phi(\boldsymbol{x}_i) \rangle - b \le \varepsilon + \xi_i^+ \\ \langle \boldsymbol{w}, \phi(\boldsymbol{x}_i) \rangle + b - y_i \le \varepsilon + \xi_i^- \\ \xi_i^+, \xi_i^- \ge 0 \end{cases}$$

where ε is the maximum tolerable error, ξ_i^+ and ξ_i^- are slack variables, $\|\cdot\|$ is the Euclidean norm, and C is a parameter that represents a trade-off between the model complexity and the tolerance to an error larger than ε. The dual form of Eq. (12) becomes

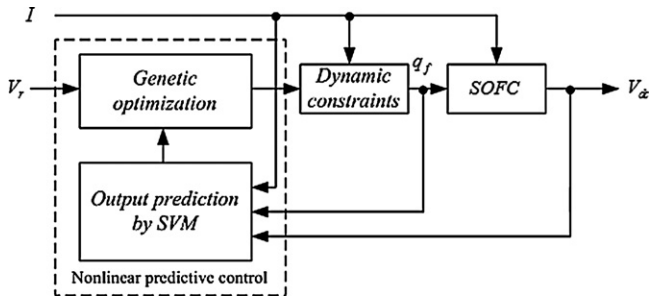

Fig. 3. Block diagram of the proposed nonlinear predictive controller.

a quadratic programming (QP) problem as follows:

$$\max_{\alpha^+, \alpha^-} \sum_{i=1}^m y_i(\alpha_i^+ - \alpha_i^-) - \frac{1}{2}\sum_{i=1}^m\sum_{j=1}^m (\alpha_i^+ - \alpha_i^-)(\alpha_j^+ - \alpha_j^-)K(\boldsymbol{x}_i, \boldsymbol{x}_j) - \varepsilon\sum_{i=1}^m (\alpha_i^+ + \alpha_i^-) \tag{13}$$

$$s.t. \; \sum_{i=1}^m (\alpha_i^+ - \alpha_i^-) = 0, \quad \alpha_i^+, \alpha_i^- \in \left[0, \frac{C}{m}\right], \quad i = 1, \ldots, m$$

where $K(\boldsymbol{x}_i, \boldsymbol{x}_j) = \phi^T(\boldsymbol{x}_i)\phi(\boldsymbol{x}_j)$ is a kernel function. Motivated by Mercer's condition, the kernel function handles the inner product in the feature space and hence the explicit form of $\phi(\boldsymbol{x}_i)$ does not need to be known.

The solution of the QP problem, Eq. (13), gives the optimum values of α_i^+ and α_i^-. One then obtains $\boldsymbol{w} = \sum_{i=1}^m (\alpha_i^+ - \alpha_i^-)\phi(\boldsymbol{x}_i)$, where some of the coefficients $(\alpha_i^+ - \alpha_i^-)$ have non-zero values and the corresponding training data points have an approximation error equal to or larger than ε. When only the support vectors corresponding to non-zero values of $\beta_i = (\alpha_i^+ - \alpha_i^-)$ are considered, Eq. (10) becomes:

$$F(\boldsymbol{x}_i) = \sum_{j=1}^l \beta_j K(\boldsymbol{x}_i, \boldsymbol{x}_j) + b \tag{14}$$

where l denotes the number of support vectors in the model. The bias b is calculated as:

$$b = -\frac{1}{2}\sum_{i=1}^m \left(\alpha_i^+ - \alpha_i^-\right)\left(K(\boldsymbol{x}_r, \boldsymbol{x}_i) + K(\boldsymbol{x}_s, \boldsymbol{x}_i)\right) \tag{15}$$

where $\boldsymbol{x}_r$ and $\boldsymbol{x}_s$ are support vectors.

5. Constrained model predictive control with a terminal cost based on genetic optimization

The structure of the proposed nonlinear predictive control is given in Fig. 3, where V_r is the set-point for the output voltage. A nonlinear SVM model is first identified to approximate the behavior of the SOFC system, and then a specially designed GA is employed to solve the resulting nonlinear constrained predictive control problem. In addition, a dynamic constraint unit is adopted in Fig. 3 in order to meet the requirements for fuel utilization and control constraints.

5.1. Identification of the SOFC system based on SVM

To achieve nonlinear predictive control, a nonlinear SVM model is used to approximate the behavior of the SOFC system.

Considering the effect of the dynamics of the SOFC system up to third order, the output of the system at sampling instance $k+1$ can be reasonably written as a function of past outputs, control inputs, and measurable disturbance inputs at the kth, $(k-1)$th, and $(k-2)$th instants. Thus:

$$V_{dc}(k+1) = F[V_{dc}(k), V_{dc}(k-1), V_{dc}(k-2), q_f(k), q_f(k-1), q_f(k-2), I(k), I(k-1), I(k-2)] = \sum_{i=1}^{l} \beta_i K(\boldsymbol{x}_i, \tilde{\boldsymbol{x}}(k)) + b \quad (16)$$

where $\tilde{\boldsymbol{x}}(k) = [V_{dc}(k), V_{dc}(k-1), V_{dc}(k-2), q_f(k), q_f(k-1), q_f(k-2), I(k), I(k-1), I(k-2)]^T$ is the input vector to the SVM model at instant k, $\boldsymbol{x}_i (i = 1, 2, \ldots, l)$ are support vectors in the model, and β_i and b are constant coefficients obtained through training.

The procedure for SVM identification of the SOFC system can be summarized as follows:

(1) A set of measured I/O data $(q_f^i, I^i, V_{dc}^i), \quad i = 1, 2, \ldots, m$ is first acquired from the SOFC system. The samples should cover the whole working range.To prevent some elements that have larger original absolute values from dominating the final kernel value, it is necessary to carry out some preprocessing of the raw data before feeding them into the SVM model. In this project, all of the feature elements and the target values have been scaled so that they fall into the range of $[-1,1]$. When using this SVM model, the computed target value should be converted back to the same scales that were used for the original target values.
(2) Next, the training samples of the SVM are organized using $\boldsymbol{x}_i = \left[V_{dc}^{i+2}, V_{dc}^{i+1}, V_{dc}^i, q_f^{i+2}, q_f^{i+1}, q_f^i, I^{i+2}, I^{i+1}, I^i\right]^T$ as the input variable and $y_i = V_{dc}^{i+3}$ as the output variable, $i = 1, 2, \ldots, (m-3)$.
(3) The parameters of the SVM, including the weighting coefficient C, the width parameter σ (a Gaussian kernel function is adopted), and ε, are set. σ and C affect the generalization ability of the SVM in opposite directions. Setting C too low will result in insufficient learning from the training data, while setting C too high will lead to overfitting.
(4) Lastly, the optimization problem, Eq. (12), is constructed and solved.

Herein, the optimization problem, Eq. (12), is practically solved by its dual problem, Eq. (13), using the sequential minimal optimization (SMO) algorithm [18,19]. The values of α_i^+ and α_i^- are then determined, and the nonlinear SVM model of the SOFC can be acquired according to Eq. (16).

5.2. Formulation of the predictive control problem for an SOFC

Because of the use of a nonlinear SVM predictive model, an NP-hard nonlinear optimization problem needs to be solved to achieve the MPC. A GA has been shown to give better performance than a quasi-Newtonian optimization technique in solving this kind of optimization problem [12]. In this study, the standard GA-based model predictive control has been modified by taking advantage of the well-developed theory on the stability of model predictive control [20–22].

The three key ingredients of a stabilizing predictive control are summarized in Ref. [20], which comprise a terminal set, a terminal cost, and a local controller. In this study, we have employed a linear quadratic (LQ) controller as the local controller and a corresponding terminal cost has been incorporated into the performance index of the standard GA-based MPC.

The performance index and the constraints of the MPC for the SOFC system are defined by:

$$J(k) = \sum_{i=0}^{N-1} \left[(\boldsymbol{x}(k+i+1|k) - \bar{x})^T \boldsymbol{Q}(\boldsymbol{x}(k+i+1|k) - \bar{\boldsymbol{x}}) + R\Delta q_f^2(k+i|k)\right] + \Psi(\boldsymbol{x}(k+N+1|k) - \bar{\boldsymbol{x}}) \quad (17)$$

$$\begin{cases} \boldsymbol{x}(k+i+1|k) = F'[\boldsymbol{x}(k+i|k), q_f(k+i|k), \boldsymbol{I}_v(k+i)] \\ V_{dc}(k) = [\,1 \quad 0 \quad 0 \quad 0 \quad 0\,]\boldsymbol{x}(k) \end{cases} \quad (18)$$

$$\tilde{q}_{f\min} \le q_f(k+i|k) \le \tilde{q}_{f\max}, \quad i = 0, \ldots, N-1 \quad (19)$$

$$\Delta q_{f\min} \le \Delta q_f(k+i|k) \le \Delta q_{f\max}, \quad i = 0, \ldots, N-1 \quad (20)$$

where N is the prediction horizon; $F'(\,.\,)$ is the state-space representation of the SVM model $F(.)$ in Eq. (16) by setting the state vector $\boldsymbol{x}(k) = [V_{dc}(k), V_{dc}(k-1), V_{dc}(k-2), q_f(k-2), q_f(k-1)]^T$; $\boldsymbol{x}(k+i+1|k)$ is the predicted state at instant $k+i+1$ based on the current state $\boldsymbol{x}(k)$ and control sequence; $\Delta q_f(k+i|k) = q_f(k+i|k) - q_f(k+i-1|k)$ is the predicted change in the control input signal; $\bar{\boldsymbol{x}}$ is the equilibrium value of the state vector corresponding to the current set-point (see (27)); $\boldsymbol{Q} = \boldsymbol{Q}^T \ge 0$, $R > 0$; $[\tilde{q}_{f\min}, \tilde{q}_{f\max}]$ are dynamic constraints to meet the requirements for fuel utilization and control constraints, which will be described in Section 5.3; and $\boldsymbol{I}_v(k) = [I(k), I(k-1), I(k-2)]^T$.

The last term in Eq. (17) represents the terminal cost. This terminal cost represents the stabilizing cost that would be required when the system is to be controlled beyond the finite-time horizon N toward the infinite-time horizon. We assume that this stabilizing controller can be designed by a fictitious local LQ controller near the equilibrium point.

The optimal cost in driving the system to equilibrium from the time instant $k+N+1$ to the infinite time is defined by:

$$\Psi(\boldsymbol{x}(k+N+1|k) - \bar{\boldsymbol{x}}) = (\boldsymbol{x}(k+N+1|k) - \bar{\boldsymbol{x}})^T \boldsymbol{P}(\boldsymbol{x}(k+N+1|k) - \bar{\boldsymbol{x}}) \quad (21)$$

where $\boldsymbol{P}$ is the symmetric positive semi-definite solution of the algebraic Riccati equation:

$$\boldsymbol{P} = \boldsymbol{A}^T\boldsymbol{P}\boldsymbol{A} - \boldsymbol{A}^T\boldsymbol{P}\boldsymbol{B}(\boldsymbol{B}^T\boldsymbol{P}\boldsymbol{B} + \tilde{R})^{-1}\boldsymbol{B}^T\boldsymbol{P}\boldsymbol{A} + \tilde{\boldsymbol{Q}} \quad (22)$$

where $\boldsymbol{A}$ and $\boldsymbol{B}$ are constant matrices of appropriate dimensions obtained by linearizing or identifying the SOFC system Eq. (1) around the nominal operation point; and $\tilde{\boldsymbol{Q}} = \tilde{\boldsymbol{Q}}^T \ge 0$ and $\tilde{R} > 0$ are the weighting matrices for the local LQ controller.

The local controller $\boldsymbol{K}_{\mathrm{LQ}}$ corresponding to the terminal cost is designed as:

$$\boldsymbol{K}_{\mathrm{LQ}} = -(\boldsymbol{B}^T\boldsymbol{P}\boldsymbol{B} + \tilde{R})^{-1}\boldsymbol{B}^T\boldsymbol{P}\boldsymbol{A} \quad (23)$$

In formulating the optimization problem, (17)–(20), we assume that there is a finite horizon length N, such that the prediction of the state vector, $\boldsymbol{x}(k+N+1|k) \in \Omega$, where Ω is the terminal set, and the constraints can be assumed to be inactive for $i \ge N$, because it is very difficult to calculate the terminal set for a given nonlinear system, and also to reduce the computational load. As a result, the terminal set constraint is omitted in (17)–(20). Note that the assumption concerning the terminal set may be met if the prediction horizon is long enough or, in the case of short horizon, a large weighting matrix $\tilde{R}$ is used in designing the local controller.

The local LQ controller is only used to determine a terminal penalty matrix $\boldsymbol{P}$ off-line and to help the GA improve the initial

population, which will be illustrated in Section 5.5. This method does not require the globally optimal input profile to be found numerically at every step. Stability only requires feasible solutions to the optimization problem. The computational (and performance) advantage of this scheme lies in the fact that shorter horizons can be used, without jeopardizing performance and stability. This is especially beneficial for on-line application of the GA-based predictive control approach.

5.3. Calculation of the dynamic constraints

We assume that the safe range of fuel utilization is within $[u_{f\min}, u_{f\max}]$, and that the actuator constraints on the control signal are $[q_{f\min}, q_{f\max}]$. The dynamic constraint unit in Fig. 3 is designed as follows.

In terms of Eq. (9), to guarantee a safe utilization, the hydrogen flow should be within $[q_{\mathrm{H}_2\min}, q_{\mathrm{H}_2\max}]$, where $q_{\mathrm{H}_2\min}(k) = 2K_rI(k)/u_{f\max}$ and $q_{\mathrm{H}_2\max}(k) = 2K_rI(k)/u_{f\min}$.

Because it is appropriate to approximate the fuel-processing unit using a first-order transfer function, we can calculate the constraints $[q'_{f\min}, q'_{f\max}]$ on the fuel flow (the natural gas flow rate) from $[q_{\mathrm{H}_2\min}, q_{\mathrm{H}_2\max}]$. For example, in the case of sample time $T_s = 1$ s, $q'_{f\max}(k) = (q_{\mathrm{H}_2\max}(k) - 0.8187q_{\mathrm{H}_2}(k))/0.1813$, $q'_{f\min}(k) = (q_{\mathrm{H}_2\min}(k) - 0.8187q_{\mathrm{H}_2}(k))/0.1813$.

The final dynamic constraints $[\tilde{q}_{f\min}, \tilde{q}_{f\max}]$ on the fuel flow can thus be calculated using:

$$\tilde{q}_{f\min} = \max(q_{f\min}, q'_{f\min}) \tag{24}$$

$$\tilde{q}_{f\max} = \min(q_{f\max}, q'_{f\max}) \tag{25}$$

5.4. Offset-free output tracking

To achieve offset-free output tracking, a simple disturbance estimator is run at each step, assuming that the state disturbance is given by the difference between the latest measured state and the previously expected state:

$$\hat{\boldsymbol{d}}(k) = \boldsymbol{x}(k) - \boldsymbol{x}(k|k-1) \tag{26}$$

This is then used to estimate the equilibrium values of the state vector $\bar{\boldsymbol{x}}$ and the fuel flow $\bar{q}_f$, assuming that the disturbance will remain constant at this estimated value: $\bar{\boldsymbol{d}} = \hat{\boldsymbol{d}}(k)$. Specifically, $\bar{\boldsymbol{x}}$ and $\bar{q}_f$ are found as the solutions to the simultaneous equations:

$$\begin{cases} \bar{\boldsymbol{x}} = F'[\bar{\boldsymbol{x}}, \bar{q}_f, \boldsymbol{I}_v(k)] + \bar{\boldsymbol{d}} \\ V_r = [\,1 \quad 0 \quad 0 \quad 0 \quad 0\,]\bar{\boldsymbol{x}} \end{cases} \tag{27}$$

Note that this results in offset-free control in the presence of an unknown but constant disturbance, even if the steady-state gains in the model are not accurate.

Another measure to achieve offset-free properties is to introduce an integration action. We assume that $\boldsymbol{x}'(k) = [\Delta V_{dc}(k), \Delta V_{dc}(k-1), \Delta V(k-2), \Delta q_f(k-2), \Delta q_f(k-1), e(k)]^T$, where $e(k) = V_r(k) - V_{dc}(k)$. The performance index is accordingly modified as:

$$J(k) = \sum_{i=0}^{N-1} [\boldsymbol{x}'^T(k+i+1|k)\boldsymbol{Q}\boldsymbol{x}'(k+i+1|k) + R\Delta q_f^2(k+i|k)] + \Psi(\boldsymbol{x}'(k+N+1|k)) \tag{28}$$

Because this method may result in integrator wind-up, this part of the contents is omitted herein.

5.5. Genetic optimization of control inputs

Due to the use of an SVM model, the proposed method formulates a dynamic nonlinear optimization problem, to which the conventional optimization techniques cannot be easily applied. Therefore, in this work, the on-line optimization problem is solved using a GA.

To deal with constraints in this optimization problem, the penalty function method is commonly used. However, this approach lowers the efficiency of a GA, because of the waste of genetic material due to unfeasible solutions stemming from standard genetic operators in the population. In this study, specially designed genetic operators have been employed to make the newly generated chromosomes satisfy the constraints automatically.

The algorithm starts with an initial population of chromosomes, which represent possible solutions of the optimization problem. The objective function is computed for each chromosome. New generations are produced by the genetic operators, which are designated as selection, crossover, and mutation. The algorithm stops after the maximum permissible time has elapsed.

A chromosome that is a candidate solution of the optimization problem is represented by s_i, the elements of which comprise present and future control inputs, and has the following structure [13]:

$$s_i = [q_{fi}(k) \;\; q_{fi}(k+1) \;\; \cdots \;\; q_{fi}(k+N-1)], \quad i = 1, \ldots, L \tag{29}$$

where k indicates the current time, and L is the number of chromosomes. The algorithm can be described as follows:

Step 1 (initial population generation): the number of iterations $iter = 1$ is set. Predictive control uses the receding horizon principle, which implies that an evolution has to be calculated at each time step. Hence, the past evolutions give important information that can be used to improve the initial population of the current evolution

The optimal input sequence obtained at $k-1$ is assumed to be $U^*(k-1) = \{q_f^*(k-1), \; q_f^*(k), \; \ldots, \; q_f^*(k+N-2)\}$. At the current time k, we consider a "shifted" input sequence $\tilde{U}(k)$ as shown below, where the last gene takes $\tilde{q}_f(k+N-1)$, obtained using the designed local controller, to be one of the initial chromosomes. This chromosome might be a very good guess for the solution of the next optimization problem.

$$U^*(k-1) = \left\{ \underbrace{q_f^*(k-1)}_{applied}, \;\; q_f^*(k), \;\; \ldots, \;\; \underbrace{q_f^*(k+N-3)}, \;\; \underbrace{q_f^*(k+N-2)} \right\}$$

$$s_1 = \tilde{U}(k) = \left\{ q_f^*(k), \;\; q_f^*(k+1), \;\; \ldots, \;\; q_f^*(k+N-2), \;\; \underbrace{\tilde{q}_f(k+N-1)}_{new\ tail} \right\}$$

where the newly added tail is defined by

$$\tilde{q}_f(k+N-1) = \begin{cases} low & \text{if } \tilde{q}'_f < low \\ \tilde{q}'_f & \text{if } low \le \tilde{q}'_f \le upper \\ upper & \text{if } \tilde{q}'_f > upper \end{cases} \tag{30}$$

$$\tilde{q}'_f = \boldsymbol{K}_{LQ}(x(k+N-1|k) - \bar{x}) + \bar{q}_f \tag{31}$$

$$low = \max\{0, q_f^*(k+N-2) + \Delta q_{f\min}\} \tag{32}$$

$$upper = \min\{1, q_f^*(k+N-2) + \Delta q_{f\max}\} \tag{33}$$

To satisfy both the control and control move constraints, we use a simple procedure to generate the remaining $L-1$ chromosomes $s_2 - s_L$ of the initial population.

(1) For the current input value:

$$q_{fi}(k) = \min(\tilde{q}_{f\max}, \max(\tilde{q}_{f\min}, rand[q_f(k-1) + \Delta q_{f\min}, q_f(k-1) + \Delta q_{f\max}])), \quad 2 \le i \le L$$

(2) For the rest of the input values:

$$q_{fi}(k+j) = \min(\tilde{q}_{f\max}, \max(\tilde{q}_{f\min}, rand[q_{fi}(k+j-1) + \Delta q_{f\min}, q_{fi}(k+j-1) + \Delta q_{f\max}])), \quad 2 \le i \le L, \quad 1 \le j \le N-1$$

In the above equations, *rand* [.] is a random number within [.], and a new random number is generated each time.

Step 2 (fitness function evaluation): the objective function of Eq. (17) is evaluated for all of the chosen chromosomes. Their fitness value is then calculated according to:

$$fitness(i) = \frac{1}{1+J_i}, \quad i = 1, 2, \ldots, L \tag{34}$$

where J_i is the value of the objective function for the ith chromosome.

The normalized fitness value of each chromosome, that is, the selection probability, is then calculated by:

$$p_i = \frac{fitness(i)}{\sum_{i=1}^{L} fitness(i)} \tag{35}$$

Step 3 (selection operation): the m_2 best individuals are retained and reintroduced into the population of the next generation. Therefore, the partly optimized chromosomes will not get lost in spite of the disruption of building blocks during crossover.

The rest of the L-m_2 chromosomes are generated according to their selection probabilities. The chromosomes with high fitness value have a greater chance of being selected.

Step 4 (crossover operation): for each chromosome, a random number r_1 between 0 and 1 is generated. If r_1 is lower than the probability of crossover p_c, this particular chromosome will undergo the process of crossover, otherwise it will remain unchanged. The selected chromosomes are paired and for each selected pair one of the following two crossover operations is implemented with equal probability

(1) The one-point crossover operation

A random integer z between 1 and $N-1$ is generated, which indicates the position of the crossing point. Two new chromosomes are produced by interchanging all of the members of the parents following the crossing point, which can be expressed graphically as follows:

$$s_i = \{q_{fi}(k), \ldots, q_{fi}(k+z-1), |q_{fi}(k+z), \ldots, q_{fi}(k+N-1)\}$$
$$s_{i+1} = \{q_{f(i+1)}(k), \ldots, q_{f(i+1)}(k+z-1), |q_{f(i+1)}(k+z), \ldots, q_{f(i+1)}(k+N-1)\}$$
$$\text{the one point crossover} \Downarrow$$
$$s_i^{new} = \{q_{fi}(k), \ldots, q_{fi}(k+z-1), |q_{f(i+1)}(k+z), \ldots, q_{f(i+1)}(k+N-1)\}$$
$$s_{i+1}^{new} = \{q_{f(i+1)}(k), \ldots, q_{f(i+1)}(k+z-1), |q_{fi}(k+z), \ldots, q_{fi}(k+N-1)\}$$

The previous operation might produce infeasible offspring if the input values at the crossing point do not satisfy the control move constraints. This situation is avoided by the following correction mechanism for each of the new chromosomes s_i^{new} and s_{i+1}^{new}, which modifies the values of the input parameters after the crossing position so that the control move constraints are satisfied.

For s_{i+1}^{new}, it is supposed that $d = q_{fi}(k+z) - q_{f(i+1)}(k+z-1)$, and then:

$$q_{fi}(k+z+j) = \begin{cases} q_{fi}(k+z+j) - (d - \Delta q_{f\max}), & \text{if} \quad d > \Delta q_{f\max} \\ q_{fi}(k+z+j) - (d - \Delta q_{f\min}), & \text{if} \quad d < \Delta q_{f\min} \end{cases}$$
$$(0 \le j \le N-z-1) \tag{36}$$

Similar equations can be obtained for the chromosome s_i^{new}.

(2) The uniform crossover operation

For the uniform crossover operation, two new chromosomes based on s_i and s_{i+1} are produced by:

$$\begin{cases} s_i^{new} = r_2 \cdot s_i + (1 - r_2) \cdot s_{i+1} \\ s_{i+1}^{new} = (1 - r_2) \cdot s_i + r_2 \cdot s_{i+1} \end{cases} \tag{37}$$

where r_2 is a random number between 0 and 1.

Step 5 (mutation operation): for every member of each chromosome, a random number r_3 between 0 and 1 is generated. If r_3 is lower than the probability of mutation p_m, this particular member of the chromosome will undergo the process of mutation; otherwise, it will remain unchanged. For the selected members, lower and upper bounds $[b_l(j), b_u(j)]$ are defined as:

$$b_u(j) = \begin{cases} \min(\Delta q_{f\max} + q_f(k-1), \Delta q_{f\max} + q_{fi}(k+1), \tilde{q}_{f\max}), & j = 0 \\ \min(\Delta q_{f\max} + q_{fi}(k+j-1), \Delta q_{f\max} + q_{fi}(k+j+1), \tilde{q}_{f\max}), & 0 < j < N-1 \\ \min(\Delta q_{f\max} + q_{fi}(k+j-1), \tilde{q}_{f\max}), & j = N-1 \end{cases} \tag{38}$$

$$b_l(j) = \begin{cases} \max(\Delta q_{f\min} + q_f(k-1), \Delta q_{f\min} + q_{fi}(k+1), \tilde{q}_{f\min}), & j = 0 \\ \max(\Delta q_{f\min} + q_{fi}(k+j-1), \Delta q_{f\min} + q_{fi}(k+j+1), \tilde{q}_{f\min}), & 0 < j < N-1 \\ \max(\Delta q_{f\min} + q_{fi}(k+j-1), \tilde{q}_{f\min}), & j = N-1 \end{cases} \tag{39}$$

The above bounds define the region of values that will produce a feasible solution. The mutation operation is then achieved by the generation of a random number within $[b_l(j), b_u(j)]$.

$$q_{fi}^{new}(k+j) = r_m(j) \quad \text{if} \quad r_3 < p_m \tag{40}$$

where $r_m(j)$ is a random number within $[b_l(j), b_u(j)]$.

Step 6 (repeat or stop): if the maximum allowed time has not elapsed, the algorithm is set and returned to **Step 2**. Otherwise, the algorithm is stopped and the chromosome that produced the highest value of the fitness function throughout the entire procedure is selected.

The previous modified GA makes it possible to calculate suboptimal control in real time.

6. Simulation results

In this section, we describe application of the proposed nonlinear predictive controller to the SOFC problem to achieve safe fuel utilization and maintain operational constraints when only the voltage output is measurable on-line. The sampling rate of the SOFC and the MPC was chosen as $T_s = 1$ s. For all simulations, the following parameters were set: $[q_{f\min}, q_{f\max}] = [0, 1.2]$ mol s^{-1}, $\Delta q_{f\max} = -\Delta q_{f\min} = 0.7$ mol s^{-1}, $[u_{f\min}, u_{f\max}] = [0.7, 0.9]$, $p_c = 0.8$, $p_m = 0.1$, $L = 20$, $m_2 = 2$, $R = 10$, $\mathbf{Q} = \tilde{\mathbf{Q}} = diag(0.1 \quad 0 \quad 0 \quad 0 \quad 0)$.

6.1. Identification of the SOFC system

Open-loop input–output data are required to train the SVM model of an SOFC system. Open-loop input–output data samples were obtained by exciting the open-loop SOFC system using designed sine signals $0.7823 + 0.3\sin(0.5t)\sin t$ and $300 + 50\sin(0.03t)\sin(0.04t)$ for the fuel and the current demand (i.e., q_f and I), respectively, which were collected over 1000 s and are plotted in Fig. 4. All 1000 of the sampled data points were divided into two sets, the training set and the testing set, where the training set contained 900 data points and the testing set contained the remaining 100 data points.

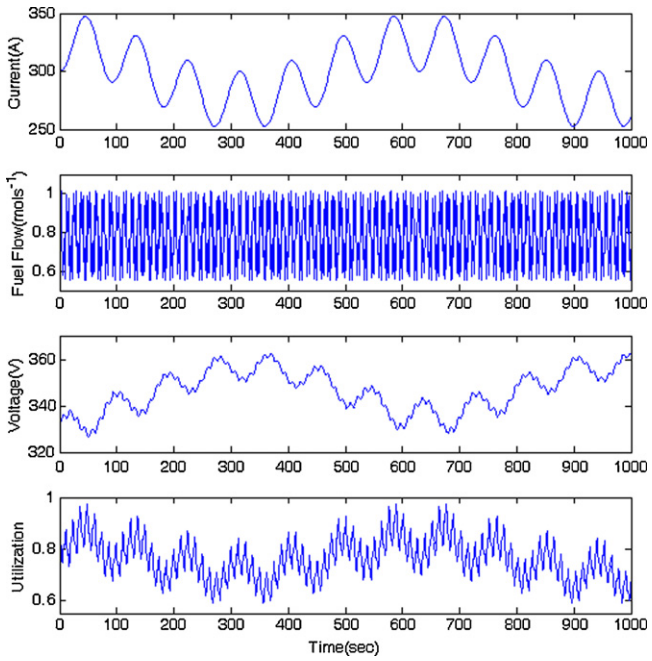

Fig. 4. Input excitation and output response signals of the SOFC.

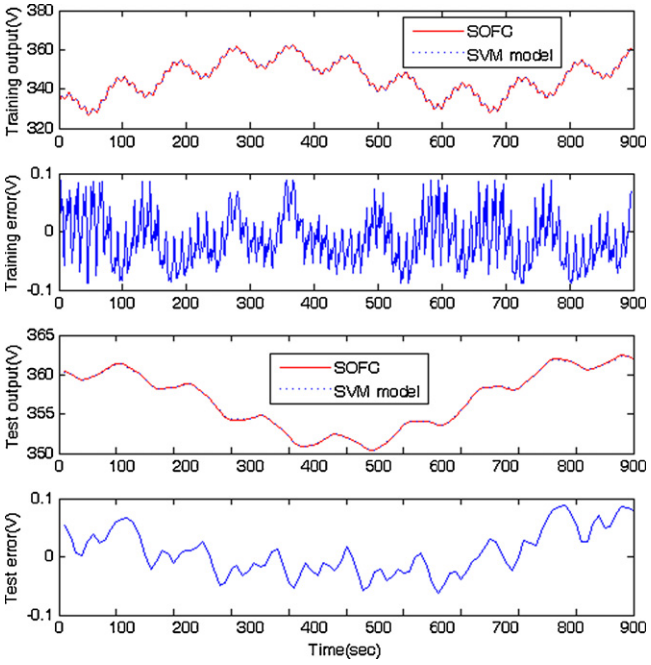

Fig. 5. Training and test results of the SVM model.

We first identified the SVM model of the SOFC system with different parameter settings, giving the results shown in Table 2. The quality of the approximation was assessed using the root-mean-square error (RMSE) between the samples and the SVM model.

In order to make a trade-off between the accuracy and the complexity of the SVM, we chose $C = 10{,}000$, $\varepsilon = 0.01$, and $\sigma = 40$ in terms of the test error and the number of support vectors in the following simulations. The corresponding training and test results are plotted in Fig. 5, which shows that the SVM can approximate the behavior of the SOFC system with good accuracy.

6.2. Predictive control of the SOFC system

By linearizing Eq. (1) around its equilibrium point, we obtained the transfer function of the SOFC system:

$$G(s) = \frac{V_{dc}(s)}{q_f(s)} = k_g \cdot \frac{\tau s + 1}{(\tau_f s + 1)(\tau_{H_2} s + 1)(\tau_{O_2} s + 1)} \tag{41}$$

where $k_g = Y_1 + Y_2$, $\tau = (Y_1\tau_{O_2} + Y_2\tau_{H_2})/(Y_1 + Y_2)$, $Y_1 = N_0R_0T_0/(2F_0K_{H_2}p_{H_2,0})$, $Y_2 = N_0R_0T_0/(4F_0\tau_{H-O}K_{O_2}p_{O_2,0})$. $p_{H_2,0}$ and $p_{O_2,0}$ denote the steady-state partial pressures of hydrogen and oxygen, respectively.

Specifically, around the nominal operation point with $q_f = 0.7023\ \text{mol s}^{-1}$, $I = 300\ \text{A}$, $V_{dc} = 333\ \text{V}$:

$$G(s) = 230.37 \cdot \frac{5.85s + 1}{(5s + 1)(26.1s + 1)(2.91s + 1)} \tag{42}$$

Table 2
Training and test results with different parameter settings.

σ	ε	C	Training error (RMSE)	Test error (RMSE)	Number of support vectors
20	0.01	10,000	0.0462	0.0454	24
40	0.01	10,000	0.0435	0.0391	16
60	0.01	10,000	0.0416	0.0411	14
40	0.02	10,000	0.0985	0.0888	14
40	0.01	1000	0.0458	0.0405	19

Converting Eq. (42) to its equivalent discrete state-space form, we obtain:

$$\begin{cases} \boldsymbol{x}(k+1) = \boldsymbol{A}\boldsymbol{x}(k) + \boldsymbol{B}\Delta q_f(k) \\ V_{dc}(k) = \boldsymbol{C}\boldsymbol{x}(k) \end{cases} \tag{43}$$

$$\text{where } \boldsymbol{A} = \begin{bmatrix} 2.49 & -2.051 & 0.5588 & -1.141 & 1.5981 \\ 1 & 0 & 0 & 0 & 0 \\ 0 & 1 & 0 & 0 & 0 \\ 0 & 0 & 0 & 0 & 1 \\ 0 & 0 & 0 & 0 & 1 \end{bmatrix},$$

$$\boldsymbol{B} = [\,1.553 \quad 0 \quad 0 \quad 0 \quad 1\,]^T, \qquad \boldsymbol{C} = [\,1 \quad 0 \quad 0 \quad 0 \quad 0\,]$$

The following positive semi-definite matrix and local controller are then calculated by Eqs. (22) and (23) with $\tilde{R} = 10,000$.

$$\boldsymbol{P} = \begin{bmatrix} 88.1 & -125.9 & 45.6 & -93.1 & 237.1 \\ -125.9 & 181 & -65.7 & 134.2 & -348.6 \\ 45.6 & -65.7 & 23.9 & -48.8 & 128.6 \\ -93.1 & 134.2 & -48.8 & 99.7 & -262.6 \\ 237.1 & -348.6 & 128.6 & -262.6 & 1219.3 \end{bmatrix}$$

$$\boldsymbol{K}_{LQ} = [\,0.0318 \quad -0.0466 \quad 0.0172 \quad -0.0351 \quad 0.1461\,]$$

To illustrate the effectiveness of the proposed nonlinear predictive controller, we assume that a load disturbance causes step changes of the current at $t = 10$ s and $t = 60$ s, respectively. Let $N = 2$. Fig. 6 shows a comparison of the closed-loop response of the SOFC system with terminal cost (solid line) and without terminal cost (dashed line). These results show that better control performance can be achieved by considering terminal cost, even though a short prediction horizon is adopted. The main advantage of adopting a short horizon is that the on-line computational burden is effectively decreased since both the number of decision variables and the number of prediction steps are reduced.

6.3. Effect of the dynamic constraints

To show the effect of the dynamic constraints, we replaced the dynamic constraints on the control input signal in Fig. 6 with the usual maximum and minimum constraints, which yielded the

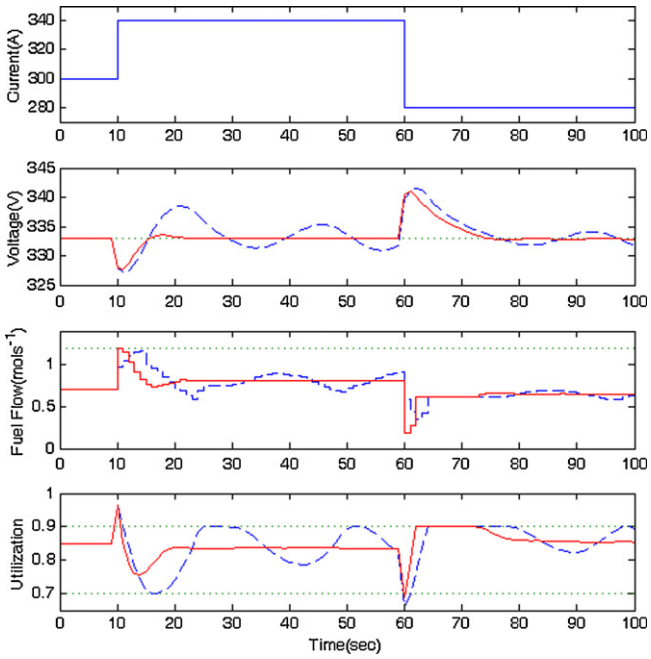

Fig. 6. Closed-loop response of the SOFC with (solid line) and without terminal cost (dashed line).

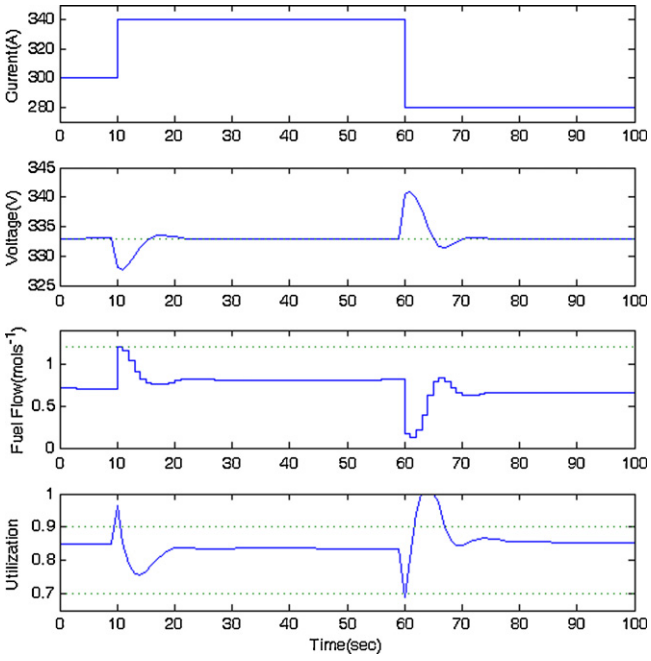

Fig. 7. Simulation results without dynamic constraints.

results shown in Fig. 7. Comparing Fig. 7 with Fig. 6, it is clear that the fuel utilization could no longer be kept within the desired safe range for the current disturbance from $t = 62$ s to $t = 67$ s without the dynamic constraints. Note that because of the slow response of the fuel flow to the output voltage and constraints on the fuel flow, the fuel utilization could not be definitely restricted to the desired range for large and sudden current load changes.

7. Conclusion

We have proposed a nonlinear predictive control strategy to solve the SOFC control problem, whereby a nonlinear SVM model is first identified to approximate the behavior of the SOFC system using an SMO algorithm, and then a specially designed GA is employed to solve the resulting nonlinear constraint predictive control problem. Meanwhile, the standard performance index has been modified by incorporating a terminal cost, which makes it possible to adopt short horizons while maintaining a satisfactory level of performance. This is especially beneficial for on-line application of GA-based predictive control. Moreover, the GA was accelerated by improving the initial population based on the optimal control sequence obtained at the previous sampling period and a local controller. Simulation results on the SOFC system have illustrated that the proposed method can successfully deal with the control and control move constraints, and that a satisfactory closed-loop performance can be achieved.

Acknowledgment

This work is supported by the National Natural Science Foundation of China (nos. 51076027 and 51036002).

References

[1] Y.H. Li, S.S. Choi, S. Rajakaruan, IEEE Trans. Energy Convers. 20 (2) (2005) 381–387.
[2] V. Knyazkin, L. Söder, C. Canizares, IEEE PowerTech Conference, Bologna, Italy, June 23–26, 2003, pp. 328–333.
[3] X. Wang, B. Huang, T. Chen, J. Process Control 17 (2) (2007) 103–114.
[4] H.B. Huo, X.J. Zhu, W.Q. Hu, H.Y. Tu, J. Li, J. Yang, J. Power Sources 185 (1) (2008) 338–344.
[5] X.J. Wu, X.J. Zhu, G.Y. Cao, H.Y. Tu, J. Power Sources 179 (1) (2008) 232–239.
[6] F. Jurado, J. Power Sources 158 (1) (2006) 245–253.
[7] X.W. Zhang, S.H. Chan, H.K. Ho, J. Li, G. Li, Z. Feng, Int. J. Hydrogen Energy 33 (2008) 2355–2366.
[8] J. Yang, X. Li, H.G. Mou, L. Jian, J. Power Sources 193 (2) (2009) 699–705.
[9] X.C. Xi, A.N. Poo, S.K. Chou, Control Eng. Pract. 15 (8) (2007) 897–908.
[10] W. Naeem, R. Sutton, J. Chudley, F.R. Dalgleish, S. Tetlow, Int. J. Control 78 (14) (2005) 1076–1090.
[11] U. Yuzgec, Y. Becerikli, M. Turker, ISA Trans. 45 (4) (2006) 589–602.
[12] S.C. Shin, S.B. Park, Electron. Lett. 34 (20) (1998) 1980–1981.
[13] H. Sarimveis, G. Bafas, Fuzzy Sets Syst. 139 (1) (2003) 59–80.
[14] C. Onnen, R. Babuška, U. Kaymak, J.M. Sousa, H.B. Verbruggen, R. Isermann, Control Eng. Pract. 5 (10) (1997) 1363–1372.
[15] M.G. Na, B.R. Upadhyaya, IEEE Trans. Nucl. Sci. 53 (4) (2006) 2318–2327.
[16] B. Schölkopf, A.J. Smola, Learning with Kernels: Support Vector Machines, Regularization, Optimization and Beyond, MIT Press, Cambridge, MA, 2002.
[17] A.J Smola, B. Schölkopf, A tutorial on Support Vector Regression, NeuroCOLT Technical Report no. NC-TR-98-030, Royal Holloway College, University of London, 1998.
[18] G.W. Flake, S. Lawrence, Mach. Learn. 46 (2002) 271–290.
[19] S.K. Shevade, S.S. Keerthi, C. Bhattacharyya, K.R.K. Murthy, IEEE Trans. Neural Networks 11 (5) (2000) 1188–1193.
[20] D.Q. Mayne, J.B. Rawlings, C.V. Rao, P.O.M. Scokaert, Automatica 36 (6) (2000) 789–814.
[21] J.M. Maciejowski, Predictive Control with Constraints, Prentice-Hall, New York, 2002.
[22] H. Chen, F. Allgöwer, Automatica 34 (10) (1998) 1205–1217.